Revista Mexicana de Física **43**, *No. 4 (1997) 600–621*

Experimental techniques in heavy ion fusion I. gamma-ray techniques

E.F. AGUILERA
Departamento de Aceleradores
Instituto Nacional de Investigaciones Nucleares
Apartado postal 18-1027, 11801 México, D.F., Mexico

Recibido el 30 de septiembre de 1996; aceptado el 4 de abril de 1997

ABSTRACT. The details of the gamma-ray technique for measuring heavy-ion fusion cross sections are described through the analysis of a particular experiment involving the $^{28}Si + ^{28}Si$ system. All steps, going from the experimental procedure and the spectra identification to the evaluation of cross sections, are thoroughly discussed. The absolute normalization method used here is shown to give accurate results in spite of the unavoidable charge collection errors, which approximately cancel in the method. Excitation functions for thirteen evaporation channels are presented, five of which had not been published before.

RESUMEN. Se describe detalladamente la técnica de rayos gamma para medir secciones eficaces de fusión, a través del análisis de un experimento particular que involucra al sistema $^{28}Si + ^{28}Si$. Todos los pasos, desde el procedimiento experimental y la identificación de espectros hasta la evaluación de secciones eficaces, son discutidos exhaustivamente. Se prueba que el método de normalización absoluta usado aquí da resultados precisos a pesar de los inevitables errores de colección de carga, los cuales se cancelan aproximadamente en el método. Se presentan las funciones de excitación para trece canales de evaporación, cinco de las cuales no habían sido previamente publicadas.

PACS: 29.30.Kv; 25.70.Jj

1. INTRODUCTION

The use of heavy ions as probes for the investigation of nuclear systems has an ever increasing importance. Although heavy ion physics started more than 40 years ago, we could say that it first flourished in the early sixties, when the high beam-quality tandem Van de Graaff accelerators were introduced. Since then, a wide range of heavy ion reactions has been studied and consequently a wealth of new information about nuclear systems has been produced (see, for example, Ref. 1). When two heavy ions collide with each other, a variety of reactions might occur depending on the masses and energies involved. The scale of time in which the reaction occurs has been used traditionally to make a first, broad classification: reactions occurring in times comparable with the time it takes for the projectile to travel a nuclear diameter are termed direct reactions,

as opposed to compound nucleus (or fusion) reactions, in which target and projectile fuse together to form a compound system that lives long enough to lose memory of all characteristics of the formation process other than those required by the conservation laws. This phenomenon, in which the nucleons of the reacting nuclei drastically re-arrange to form a compound nucleus, has captured the interest of many nuclear physicists over a number of years.

There are several ways to determine the experimental fusion cross sections for heavy ion systems. For instance, the heavy fragments resulting from the decay of the compound nucleus can be directly detected or the gamma rays emitted by these fragments, which are not usually created in their ground states, can be measured. Another way is through the detection of characteristic X-rays originating from converted electromagnetic transitions in the residual nuclei [2]. The first two methods, with which this author has been familiar for a number of years, are described in this work. Since the corresponding experimental procedures have an almost null overlap, it seemed a good idea to divide the material into two separate, selfcontained papers, which will hopefully have the advantage of facilitating the task of keeping the reader's mind on focus all the time. The first method mentioned above, usually referred to as a particle detection technique, will be dealt with in the second paper [3]. In this first part of the work we review the second method, commonly known as the γ-ray technique. Originally, this technique was developed in nuclear spectroscopy studies in heavy nuclei ($A > 100$) at relatively low energies [4], where the predominant decay mode of the compound nucleus is by multineutron evaporation because the high Coulomb barriers strongly inhibit the emission of charged particles [5]. Here, the observed strong dependence of the number of evaporated neutrons upon bombarding energy works as a selection mechanism to isolate the isotope to be studied, leading thus to relatively simple γ-ray spectra. This is not the case for lighter nuclei ($A < 80$), where the lower Coulomb barriers allow proton and α-particle emission to compete with neutron emission so that several residual nuclei (typically of the order of 10) can be formed with comparable cross sections, making more complex the problem of identifying the different γ-ray lines in the spectra.

In 1969 Nomura *et al.* [6] studied in a systematic way the complete γ-ray spectra for several light heavy-ion systems. Since then, a variety of experiments of this kind have been performed and the power of the method has been well established (see, for example, Refs. 7 and 8). In this work the γ-ray technique is thoroughly illustrated through a detailed analysis of an experiment to measure the fusion cross sections for the $^{28}\mathrm{Si} + {}^{28}\mathrm{Si}$ system. The physics resulting from this experiment has been discussed elsewhere [9] but here we will be concerned only with the details of the experimental technique from a pedagogical point of view.

In Sect. 2 the experimental procedure is described, while the main concepts used in the identification of spectra are mentioned in Sect. 3. Section 4 is devoted to give a description of the whole process of evaluation of cross sections, going through the efficiency calibration to the relative and absolute normalization of the data. The possible effects of anisotropies in the angular distributions of γ-rays and some corrections that must be made to the cross sections are discussed in Sect. 5 and 6, respectively. In Sect. 7 the results of the experiment are presented, including a discussion about the possible Doppler-shift effects. Finally, the conclusions of this work are given in Sect. 8.

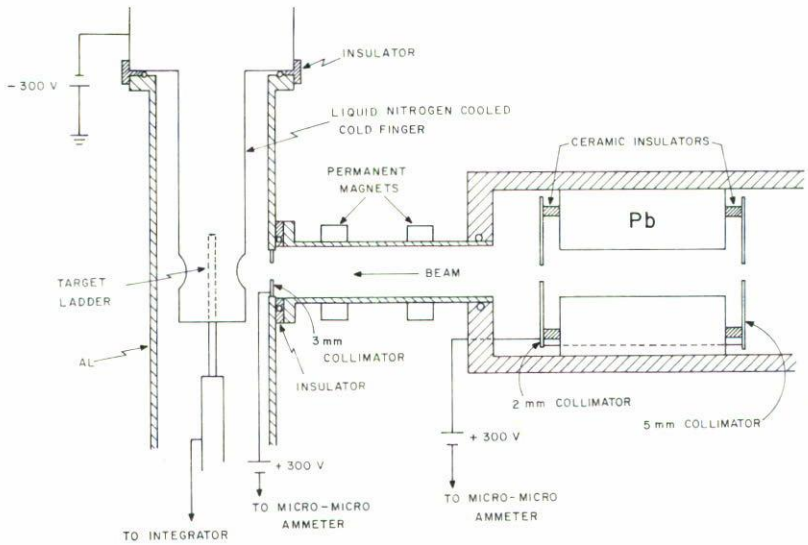

FIGURE 1. Experimental setup.

2. EXPERIMENTAL PROCEDURE

A schematic diagram of the typical experimental setup is presented in Fig. 1. As shown there, the beam collimators and cold finger are suitably biased in order to supress electrons knocked out by the beam. Sometimes a metallic screen (not shown) is introduced between the finger and the chamber wall, in which case the supressor voltage is applied to the screen instead of the finger. With this modification, the charge carried by the beam can be collected not only at the target but also at the finger which is electrically connected to the target, thus making a better Faraday cup which gives a more precise charge collection.

In addition, the beam currents on the three beam-defining collimators (the first two connected together and the chamber collimator independently) are monitored and minimized in each experimental run while simultaneously maximizing the beam on target. Due to the large production of secondary electrons that usually results when using heavy ion beams, those currents are typically negative and by minimizing them the amount of beam striking the collimators is also minimized. With this procedure, fewer secondary electrons are present to affect the charge collection and at the same time the γ-ray background due to beam-collimator reactions is reduced.

The target, made by vacuum evaporation of enriched ^{28}Si (99.9%), was deposited onto a thick gold backing which stops the reaction products without producing undesirable nuclear reactions, thus effectively controlling possible Doppler shift effects in the measured γ-rays [10]. In order to prevent oxidation, the silicon film was then covered with a thin gold layer. The ^{28}Si beam was obtained with the Tandem Van de Graaff accelerator at the University of Notre Dame, the laboratory energies ranging from 58 to 99.5 MeV, with steps of 500 keV. A Ge(Li) detector (90 cc), placed at 3.7 cm from the target and at 125° to the beam, was used to determine the total yields of γ-rays. In order

to have a better understanding of the spectra, an investigation of Doppler shift effects was done by placing the detector at the symmetric angle 55° and recording spectra for five different bombarding energies.

3. SPECTRA IDENTIFICATION

The primary task in the analysis of data consists of making a reliable identification of the γ-ray lines observed in the experiment. For a given reaction, one starts out by making a reasonable guess about what residual nuclei could be expected. The underlying consideration here is that, as experience has shown, the highly excited compound nucleus will deexcite by emitting first a few particles (combinations of neutrons, protons, and α particles) until a residual nucleus is reached in which γ-ray emission is the dominant decay mode. With this in mind, a set of the more probable residual nuclei can be fixed and the γ-ray energies reported for them in the literature [11] can be compared to the ones observed in the experiment, until all have been appropriately matched.

Besides the reported γ-energies, two more items of information provide, in some cases, additional help in identifying spectra. These are the reported branching ratios, when available, and the β-decay schemes of unstable residues. The first of these are useful when a given nuclear level, which appears as a candidate to be populated in the reaction, has been reported to decay by two or more different γ-ray transitions, each one with an appreciable branching ratio. If this is the case, the absence of one or more of these γ-rays in the spectrum will definitely rule out the level as a possible candidate, while a discrepancy in the ratio of intensities will probably indicate a contamination of at least one of the involved lines.

To illustrate how a β-decay scheme can be helpful in identifying a γ-ray spectrum, we reproduce in Fig. 2 the decay chain for ^{48}Cr. Both, ^{48}Cr and ^{48}V were positively identified as products of the reaction ^{28}Si + ^{28}Si with the help of this scheme, in the following manner: after having bombarded the target for a reasonably long time, a spectrum was taken starting immediately after the beam was shut off. The lines at 116, 308, 1312, and 984 keV seen in this spectrum, clearly indicated the presence of ^{48}Cr and possibly ^{48}V as products of the reaction (see Fig. 2). The reason for these lines being seen in the beam-off spectrum relies, of course, on the long lifetimes for β-decay, as indicated in Fig. 2. The identification was confirmed when several lines were found for each nucleus in the beam-on spectra. This kind of double-check identification was made whenever it was possible, *i.e.*, whenever a line seen in the beam-off spectrum corresponded to a β (or EC) decay of a reaction product. The other useful feature of a no-beam spectrum is that it allows one to determine the background radiation and make corrections for it if necessary.

In addition, when searching for possible levels to be populated in a given nucleus, a good guide is provided by the experimental fact that, in heavy ion reactions, high spin states are usually favored. An explanation for this can be given in terms of the same kind of arguments that we shall mention later when discussing the effects of anisotropies upon the angular distributions. The thing to do then is to look first at the levels lying at, or close to, the Yrast line, leaving aside the low angular momentum states. This

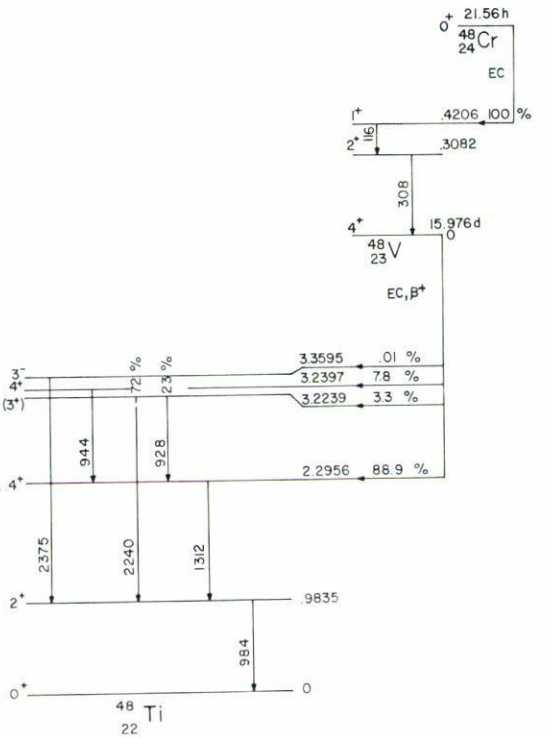

FIGURE 2. Decay chain for ^{48}Cr.

general tendency to favor high spin states was confirmed in our experiment. Finally, an additional insight into the identification is given by the experimental excitation functions, which will peak at higher energies the more (and/or the heavier) the particles that are evaporated.

The application of the criteria described above will usually lead to a very reliable identification of the experimental γ-lines. In some cases, however, serious doubts might still remain and a different sort of experiment must be done to help in the identification. A γ-γ coincidence experiment, for example, could do the job. For our ^{28}Si + ^{28}Si experiment this was not necessary.

4. EVALUATION OF CROSS SECTIONS

The next step is to determine the areas of those peaks that correspond to ground-state transitions in the residual nuclei of interest. The sum of the yields of these transitions in a given nuclide, corrected for the efficiency of the γ-ray detector, gives the total production yield for that nucleus. The cross sections must then be calculated according to the expression

$$\sigma = \frac{A}{\epsilon N_p \eta_T}, \tag{1}$$

where A is the number of counts in, or area of, the peak of interest, ϵ is the absolute peak efficiency of the detector system, N_p is the number of projectiles that struck the target, and η_T is the number of target nuclei per unit area. The determination of each of the three quantities in the denominator of this expression deserves some explanation:

4.1. EFFICIENCY CALIBRATION

The absolute peak efficiency is defined [12, 13] as the probability of recording in the detector, within the characteristic peak, a gamma-ray photon emitted from a specific source. In order to obtain this efficiency, γ-ray sources of known activity may be placed at the position of the target without otherwise changing the geometry used in the experiment. Since the emission from these sources is isotropic, the efficiency for a given γ-line is simply the ratio of the numbers of detected to emitted photons of the corresponding energy. We used several calibrated sources from an Amersham γ-ray reference source set model No. QCR.1. These, along with the respective γ-lines analyzed, are listed in Table I. Note that a non-calibrated source [^{56}Co, homemade through the ^{56}Fe(p,n) reaction] was also used in order to have a better determination of the overall behavior of the efficiency as a function of the γ-energy. The data points were fitted to a semiempirical expression which is a variant of the McNelles-Campbell formula [14] for the efficiency of a Ge(Li) detector:

$$\epsilon = a_1 \left(E_\gamma^{a_2} + a_3 e^{E_\gamma a_4} \right), \tag{2}$$

which allows us to calculate the efficiency for any γ-energy desired. In this expression ϵ is the efficiency for a given γ-energy E_γ and $a_1, \ldots, a_4$ are parameters to be determined from the fit to the data points. A fifth parameter was used to normalize the yields from the uncalibrated source to those from the calculated ones. A plot of a typical efficiency function is shown in Fig. 3.

4.2. RELATIVE NORMALIZATION

The number of projectiles (N_p) striking the target can be calculated from the total charge deposited on the target (or on target + finger) during the measurement. Division of this quantity by the charge carried by a single ion in the beam should give the desired number N_p. However, when the projectile is a heavy ion as in our case, the procedure presents complications because these ions can easily knock out electrons from whatever they strike, thus making it difficult to measure the real charge incident with the beam.

In spite of the care taken to supress electrons in these experiments, the measured charge always presents deviations with respect to the value corresponding to the true number of particles arriving at the target. These deviations can be appreciated in Fig. 4, where the excitation functions for three lines resulting from Coulomb excitation of the Au backing in the target are shown. Since the excitation functions for Au Coulomb excitation are known to be smooth curves in this energy range, the observed fluctuations must be related to errors in the process of charge collection.

The correction of these errors is accomplished by fitting one of the mentioned excitation functions to a smooth curve, which can then be used to obtain point-to-point

TABLE I. γ-ray sources and respective lines used for the determination of the efficiency of our detection system.

Source	E_γ (keV)	Intensity (γ/s/100 disint.)	Uncertainty (%)	Absolute activity during experiment (μCi)
^{60}Co	1173	99.86	1.9	9.81
	1333	99.98	1.9	
^{88}Y	898	93.2	5.0	0.57
	1836	99.4	5.0	
^{137}Cs	662	85.1	3.7	10.64
^{133}Ba	276	7.1	4.8	10.74
	303	18.7	4.8	
	356	61.9	4.8	
	384	8.9	4.8	
^{57}Co	122	85.2	4.4	3.24
	136	11.1	4.4	
^{56}Co		Rel. intens.		uncalibrated
	846.8	100.0±1.0		
	1037.8	14.04±0.14		
	1175.1	2.28±0.02		
	1238.3	66.4±0.7		
	1360.2	4.24±0.04		
	1771.0	15.65±0.16		
	2015.2	3.09±0.05		
	2034.7	7.95±0.12		
	2598.4	17.34±0.26		
	3201.9	3.18±0.10		
	3253.4	7.79±0.24		

correction factors for the collected charge. In Fig. 5, a series with the first five Hermite polynomials has been used to smooth out the excitation function for the line at 547 keV and the resulting correction factors have been used to recalculate the other two excitation functions. The correction is clearly consistent for the three lines, thus confirming the reliability of the method. The correction factors obtained this way (say f_i for the i^{th} data point) were then used in the calculation of the cross sections for the lines of interest in the ^{28}Si + ^{28}Si reaction ($N_{p_i} = f_i Q_i/ze$). This relative normalization method can be used for all reactions studied with the γ-ray technique as long as a heavy element is used for the target backing.

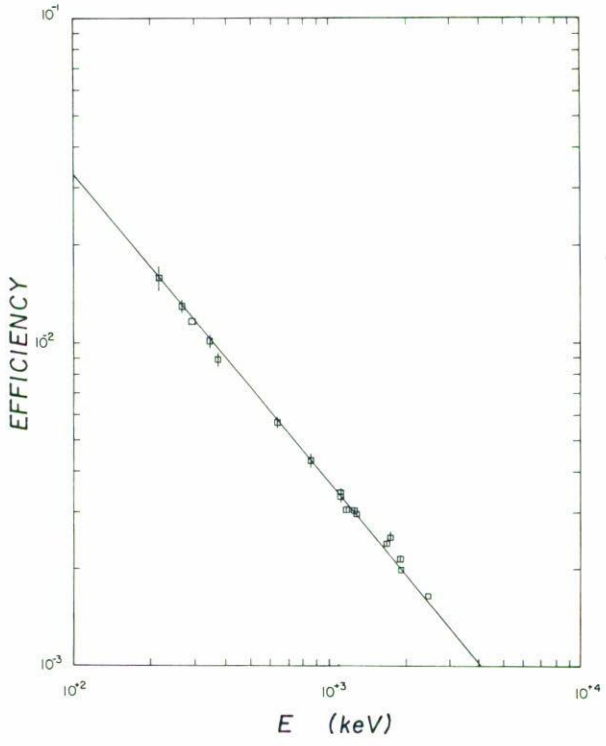

FIGURE 3. Typical efficiency function for the Ge(Li) detector.

4.3. ABSOLUTE NORMALIZATION

The last factor needed in Eq. (1) to evaluate the cross sections is the target thickness η_T, which can be thought of as a scale factor that provides the absolute value for each measured excitation function. A single absolute value for the cross section of one line, with good statistics, should be enough to determine this scale factor, which must be the same for all the runs in a given experiment. It is desirable, however, to have more than one absolute cross section value since this would allow one to check the self-consistency of the data. With this in mind, a series of experiments was devised which allowed us to make such checks not only for the final result, but also for the several intermediate steps involved in the process. The idea of the method is to start with a nuclear reaction where the values of the fusion cross sections are well-known, and use appropriate combinations of targets and projectiles to scale the relevant cross sections to these values.

The method is illustrated in Table II, where the reactions involved in the absolute normalization of $^{28}Si + {}^{28}Si$ are summarized. In some cases it is possible to use more than one line in a given reaction to make the analysis. This and the fact that several bombarding energies were used in most of the cases allowed us to make the previously mentioned self-consistency checks. In order to have good reliability, several criteria were imposed upon any γ-ray line chosen for the analysis: (i) It must have a reasonably large area to ensure statistical accuracy; (ii) It must be a well isolated peak since any slight overlap would be a source of error; (iii) It must be carefully checked that the peak is

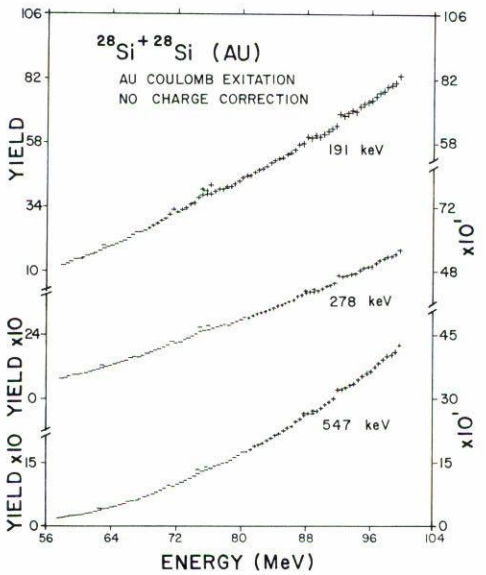

FIGURE 4. Excitation functions for lines in gold. The deviations from a smooth behavior illustrate the experimental errors in the collected charge.

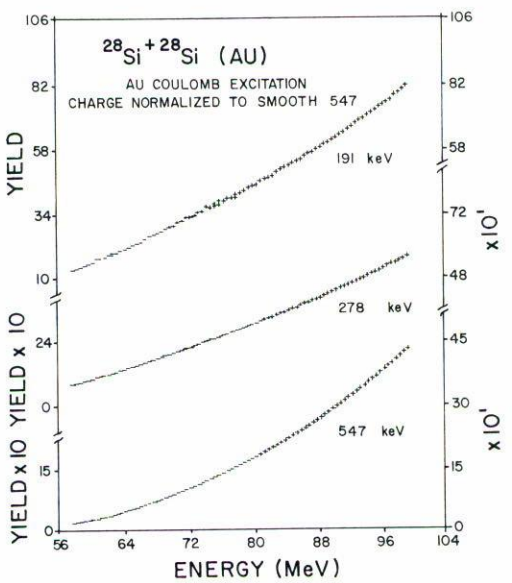

FIGURE 5. Same as Fig. 4, but the collected charge has been corrected to give a smooth behavior for the 547 keV line.

not contaminated with radiation coming from some radioactive nuclide present during the experiment; and (iv) It must also be checked that the line is free from γ-rays coming from reactions of the projectile with any possible contaminant of the target, or with the collimators. The actual γ-lines used to normalize $^{28}Si + ^{28}Si$ are indicated in Table II.

TABLE II. Experiments performed to determine the absolute normalization for the $^{28}Si + ^{28}Si$ system, based on the cross section values measured by Kolata *et al.* [15] for $^{16}O + ^{12}C$.

Projectile	E_{cm} (MeV)	Target	γ-ray lines analyzed (keV), and expected result of the analysis
^{16}O	19.3, 22.7, 24.9	^{12}C	1634(^{20}Ne)
			Target thickness
^{28}Si	21, 24, 27	^{12}C	3162(^{35}Cl)
			σ_{abs} for $^{28}Si+^{12}C$
^{12}C	21, 24, 27	^{28}Si	3162(^{35}Cl)
			Target thickness
^{28}Si	35	^{28}Si	1021(^{49}V) and 1251($^{53}Mn+^{51}Mn$)
			σ_{abs} for $^{28}Si+^{28}Si$

From the experimental point of view, this method of absolute normalization has the advantage that the same experimental setup is used for both, the normalization and the actual measurement of excitation functions. Its disadvantage is that it still relies heavily on the absolute charge collected from the beam. Some cancellation of errors might be expected, however, as can be shown in the following way: The scaling factor involved in the normalization of Table II can be written in terms of the relevant experimental quantities if we assume, for the purpose of this discussion, that only one data point is used in each reaction (*i.e.*, one γ-ray line at a given bombarding energy). We denote by Y the total yield A/ϵ in formula (1) and use repeatedly this formula to get

$$\sigma_{SiSi} = \frac{Y_{SiSi}\, Y_{SiC}}{Y_{CSi}\, Y_{OC}} \frac{N_p(CSi)\, N_p(OC)}{N_p(SiSi)\, N_p(SiC)}\, \sigma_{OC}\,, \tag{3}$$

where the subindices indicate the corresponding reaction in Table II. Since the beam striking the entrance collimators was always minimized, we might expect the main source of error in the charge collected to be the secondary electrons that, being knocked out from the target and target backing, escape from the charge collection device with the effect of artificially enhancing the positive charge collected. It is reasonable to expect that the enhancing factor will be similar for different beams under similar focusing conditions if the same charge-collection device is used. If all these factors were the same for the reactions in Table II, the errors in the charge collected would exactly cancel in Eq. (3), where the N_p's are proportional to the measured charge. In any case, some error cancellations might be expected in Eq. (3) from the fact that these errors are always biased in the same direction.

To check this expectation, the following independent method was used here to determine N_p: since all the targets involved in the normalization had a thick gold backing, some γ-ray lines corresponding to Coulomb excitation of the Au were always present. The yields expected for these lines, normalized by the number of projectiles, can be calcu-

TABLE III. Numbers of projectiles in the reactions of Table II as obtained from the collected charge Q and from the measured and calculated yields for Coulex of the line at 547 keV in Au (All targets were thin foils deposited onto a thick Au backing).

Reaction	E_{lab} (MeV)	Projectile charge state	$N_p \times 10^{-13}$ (a) using Q	$N_p \times 10^{-13}$ (b) using Coulex	$\frac{N_p(\text{Coulex})}{N_p(Q)}$
$^{16}O+^{12}C$	45	6	2.12	2.03	0.96
	53	6	2.01	1.82	0.91
	58	6	2.13	1.88	0.88
$^{28}Si+^{12}C$	70	8	4.56	4.23	0.93
	80	9	3.60	3.35	0.93
	90	10	2.11	1.90	0.90
$^{12}C+^{28}Si$	30	5	2.26	2.00	0.88
	34.29	5	2.22	1.90	0.86
	38.57	5	2.97	2.32	0.78
$^{28}Si+^{28}Si$	70	9	3.48	2.99	0.86

(a) 2% statistical error (possible systematic errors not included).

(b) 0.8% maximum statistical error estimated (possible systematic errors not included).

lated within the theoretical frame of Coulomb excitation if the relevant transition matrix elements are known [16]. It has been shown [17] that the predictions of a thick target Winther-deBoer multiple Coulomb excitation program (code SWHET, obtained from Dr. R.O. Sayer, Oak Ridge) for lines in Au are in good agreement with the γ-yields obtained with our technique. Calculations of this kind for the line at 547 keV in Au, in conjunction with the actual yields measured for this line in the experiments of Table II, provided a method to evaluate the N_p's appearing in Eq. (3) which is independent of the collected charge. The results of the two methods are compared in Table III, whose last column gives the corresponding ratios.

The first thing to notice in Table III is that the results obtained from the collected charge are systematically higher than the corresponding value derived from the Coulex calculation. This is consistent with our expectation that the collected charge will always be enhanced by the effects of the secondary electrons escaping from the charge collection device. We also note that the numbers in the last column for the O and C beams seem to indicate a systematic decrease with energy of the ratios of N_p's, in contrast with previous observations for ^{14}N beams [17] implying no energy dependence for these ratios (nothing can be said about the ^{28}Si beam since the energy and charge state both were varied in this case). However, we do not have evidence enough to draw a definite conclusion. Instead, we go on to the results obtained for the absolute cross sections indicated in Table II when consistently using any one of the two methods to calculate N_p (4th or 5th column in Table III).

TABLE IV. Comparison of absolute cross sections obtained from the two different methods used to determine the numbers of projectiles (see Table III).

Reaction	E_{cm} (MeV)	γ-ray energy (keV)	σ_{abs}(mb) using N_p(Q)	σ_{abs}(mb) using N_p(Coulex)
$^{28}Si+^{12}C$	21	3162(^{35}Cl)	90.3 ± 3.1	89.2 ± 2.5
	24	3162(^{35}Cl)	135.4 ± 4.5	133.5 ± 3.5
	27	3162(^{35}Cl)	157.4 ± 5.4	160.0 ± 4.5
$^{28}Si+^{28}Si$	35	1021(^{49}V)	46.7 ± 2.4	45.4 ± 2.6
	35	1251($^{53}Mn+^{51}Mn$)	73.9 ± 3.0	72.0 ± 3.4

Table IV shows such results not only for the reaction of interest ($^{28}Si+^{28}Si$) but also for the $^{28}Si+^{12}C$ reaction which is needed as an intermediate step in the normalization. A cancellation of errors is expected here also, as can be shown easily from the two-step equivalent of the four-step scaling formula (3). The target thicknesses were taken as the averages of the corresponding values obtained from the spectra at three different bombarding energies (see Table II), and their errors were estimated from the deviations with respect to that average rather than from propagation of statistical errors which would not take into account possible systematic biases in the peak integrations, or other non-statistical errors. The uncertainties assigned in Table IV are the combination of these errors in the target thickness with those in the γ-ray yields, efficiencies, and numbers of projectiles.

The two values obtained for the thickness (corresponding to the two methods of determining N_p) differed by 8% for the C-target and by 16% for the Si-target, in accordance with the average ratios of N_p's obtained for the first and third reactions in Table III. The corresponding cross sections, however, all agreed within errors as shown in Table IV. Actually, the individual errors assigned are always much larger than the differences between the two cross section values. These results strongly support the expectation of Q-error cancellations, giving us more confidence in our method of determining the absolute normalization.

The last two numbers in either column 4 or column 5 in Table IV were used to calculate the absolute normalization factor for our data, the results being the same for the two methods, within 2%. An uncertainty of about 5% was obtained for both cases by combining the respective listed errors. It is worth mentioning, though, that the two numbers obtained in each case, which were then averaged to get the final result, differed one from the other by only 0.4% and 1% for the Q and Coulex methods, respectively. This, along with the 2% result mentioned for the difference between the two methods, indicates a possible overestimation of the errors listed in Table IV. Using, however, the 5% estimated error, we obtain the total uncertainty in the absolute normalization by adding it quadratically to the 7% uncertainty estimated [15] for the cross sections in O+C, which we used as standards in our scaling procedure. The total uncertainty is therefore 9%. This must be considered as an estimation of the maximum systematic error in our cross section values, in the sense that it is attached to a factor multiplying all the points in each excitation function rather than to each individual point.

5. EFFECTS OF ANISOTROPIES

The use of Eq. (1) to extract a total (angle integrated) cross section from a measurement with a detector placed at a given angle is strictly correct only if the angular distribution of the emitted γ-rays is isotropic, which is not the case for heavy ion induced reactions.

A simple argument can be given to understand this last fact: taking the beam direction as the axis of quantization, the orbital angular momentum brought in by the projectile, being perpendicular to the incident direction, has only an $m = 0$ component. For fusing nuclei with non-zero spin, this δ distribution in m will be broadened, but only slightly since the average orbital angular momentum carried in by heavy ions is usually much higher than the ground state spins encountered in nuclei. The evaporated particles from this aligned compound nucleus will carry away only small amounts of angular momentum, in approximately random directions, so that the residual nuclei will be left in excited states which are also characterized by a magnetic substate distribution peaked around $m = 0$.

It is well known from the theory of electromagnetic radiation in nuclei that the γ-rays emitted from aligned states have an angular distribution which is not isotropic [18]. It can be expressed in terms of a Legendre polynomial series in $\cos\theta$ with θ being the angle between the emitted radiation and the beam direction:

$$\sigma(\theta) = A_0 \left[1 + \sum_{\mathrm{k}=1} a_{2\mathrm{k}} P_{2k}(\cos\theta) \right], \tag{4}$$

where A_0 is a normalization constant and the coefficients a_{2k} could be calculated [18–20] from the spins of the initial and final states and the multipolarities and mixing ratios of the radiation if the population distribution of the magnetic substates of the initial state is known. We will not be concerned here with these kinds of calculations, but will consider the a's as phenomenological parameters that might be determined from appropriate experiments. We just note that the maximum value of k in Eq. (4) is restricted by [19]

$$k_{\max} = \min(J_1, L), \tag{5}$$

where J_1 is the spin of the initial state and L is the multipolarity of the radiation. In practice, it is rare to find multipole radiation of higher order than 2 among the low-energy states of nuclei so that, for most practical purposes, Eq. (4) will include at most up to P_4 terms.

Coming back to the initial problem posed in this Section, we can use Eq. (4) and the orthogonality properties of the Legendre polynomials (plus the fact that $P_0 = 1$) to write an expression for the total cross section for emission of a given γ-ray line:

$$\sigma \equiv \int_{4\pi} \sigma(\theta)\, d\Omega = 4\pi A_0 . \tag{6}$$

The problem of obtaining σ reduces then to that of finding the coefficient A_0 in Eq. (4). We did this by placing our detector at $\theta = 125°$, which (rounded off) is a zero of $P_2(\cos\theta)$. The differential cross section at this angle is then written as $\sigma(125°) = A_0[1 - 0.39a_4]$.

At this point we had to rely on the existing systematics on heavy-ion induced fusion-evaporation reactions, which indicates that a_4 is in most cases a small number (see I.4 in Ref. 11 and 21), and neglected the term $0.39a_4$ in $\sigma(125°)$. Within this approximation, A_0 and therefore σ can be obtained from a single measurement at 125° and the use of expression (1) is justified.

6. CORRECTIONS TO THE CROSS SECTION

6.1. CORRECTIONS FOR TARGET CONTAMINATION

Soon after the experiment was started it became clear that some contaminant was present in our target. For instance, the observed presence of ^{39}K and ^{42}Ca in the experiment ^{28}Si+ ^{28}Si could hardly be explained as being the product of the decay of the compound nucleus ^{56}Ni by the usual mechanism in this region of mass and energy (evaporation of light particles). Their presence would be much easier to explain in terms of reactions of the ^{28}Si projectiles with ^{16}O (compound nucleus ^{44}Ti), an element that can easily combine with the Silicon in the target. Comparison of a spectrum for ^{28}Si+^{16}O at 75 MeV with the one at the same energy for ^{28}Si+ ^{28}Si, confirmed our guess of target contamination with oxygen. Since some of the lines of interest in our experiment turned out to be contaminated with γ-rays coming from reactions with ^{16}O, it was necessary to measure the reaction ^{28}Si+^{16}O, at the same energies as in the original experiment, in order to correct the data. A Ta_2O_5 target was used for this purpose.

The correction made involves the following steps:

(i) A γ-ray line from Si+O is chosen to find the scaling factor for the excitation functions from the Ta_2O_5 target to the Si (O-contaminated) target. This line, observed when using either target, must be clean in both cases and should actually satisfy the same requirements imposed upon the lines used in the absolute normalization experiments; note that in this case Si would be considered as a contaminant for the purpose of applying criterion iv) of section 4.3. The appropriate ratio of the excitation functions gives the desired scaling factor. The line at 756 keV (^{39}K+^{36}Ar) in ^{28}Si+^{16}O was used to calculate the scaling factor.

(ii) The contribution from Si+O to a given line in Si+Si is found from the corresponding excitation function for the Ta_2O_5 target by using the scaling factor found in step (i).

(iii) This contribution is subtracted from the contaminated excitation function in Si+Si, thus obtaining the corrected curve.

6.2. CORRECTIONS FOR ACTIVITY CONTAMINATION

There are always radioactive elements present in the environment around the detector which produce γ-rays. They are members of the decay chain of some very long lived isotopes such as ^{40}K (1.28×10^9 Y) or ^{232}Th (1.41×10^{10} Y). As was mentioned before, identification and quantification of this background activity can be done with the help of a spectrum taken without having beam on the target. The γ-ray activity for a given line resulting from one of these decay chains is just the yield (efficiency corrected) measured for that line in the beam-off spectrum, divided by the time (live time, *i.e.*, time corrected

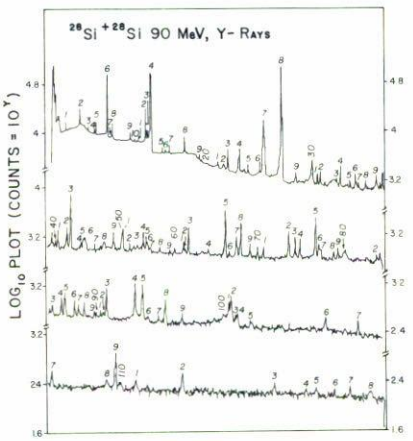

FIGURE 6. γ-ray spectrum obtained at 90 MeV bombarding energy in the ^{28}Si+ ^{28}Si experiment. The peaks are numbered in order of increasing energy and the corresponding identification is given in Tables V and VI.

for dead time of the ADC) during which the spectrum was taken. This activity, which might quite reasonably be assumed to be a constant throughout the whole experiment, in conjunction with the live-times corresponding to each spectrum in this experiment, can be used to make the pertinent correction in the event that the mentioned activity is contaminating one of lines of interest of the actual reaction. This type of correction could amount to an appreciable fraction of a given line if the cross section for this line is not very big, but we never had a considerable correction for this effect with respect to the total cross section.

The other kind of activity present during the experiment, the one arising from the β-decay of unstable residues, is much more difficult to quantify since its time dependence is in general very sensitive to the detailed history of the experiment (the beam-current on target would have to be known as a function of time not only when data are being taken but throughout the whole experiment). Only if the life-time of the radioactive residue is short compared to the typical bombarding time (time required to obtain a spectrum for a given energy) can a simplification be expected, since in this case the activity present at a given stage in the experiment will depend only on what happened in the near past and a simplified expression can then be derived [8]. Such an expression was used, for example, to estimate the possible contribution of the decay (β^+, 1.74 m) ^{50}Mn(5^+) $\rightarrow ^{50}$Cr to the excitation function for ^{50}Cr in the ^{28}Si+ ^{28}Si reaction.

7. RESULTS

A spectrum taken at 90 MeV bombarding energy is presented in Fig. 6 as an example of the data obtained. The inherent complexity of the spectrum, associated with the rather large number of residues observed from ^{28}Si+ ^{28}Si, was further increased by the lines coming from reactions with the oxygen contamination of the target. These lines were identified with the help of actual spectra from ^{28}Si+^{16}O taken with a Ta_2O_5 target, as

TABLE V. γ-ray lines observed in the $^{28}Si+^{28}Si$ experiment, as shown in Fig. 6.

No.	E_γ (keV)	Source	Notes	No.	E_γ (keV)	Source	Notes
1	108	u		30	608	^{50}Cr	$+^{214}Po$(c)
2	137	^{181}Ta	a	31	620	^{52}Mn	
2a	146	^{54}Fe	e	32	626	^{48}V	
3	154	^{49}V	$^{49}Cr(\beta^+, EC)$	33	660	^{50}Cr	
4	166	^{181}Ta	a	34	668	$^{197}Au+^{38}Ar$	b+d, resp.
5	168	^{41}Ca	d, +activity	35	689	^{49}Cr	
6	191	^{197}Au	b	36	700	^{53}Fe	
7	199	^{48}V		37	707	^{41}K	d
8	201	^{197}Au	b	38	721	^{51}Mn	
9	237	^{51}Mn	$+^{212}Bi$(c)	39	743	^{52}Cr	$^{52}Mn(\beta^+, EC)$
10	246	^{41}K	d	40	751	^{48}Cr	
11	251	^{39}K	d	41	756	$^{39}K+^{36}Ar$	d
12	268	^{197}Au	b	42	774	$^{38}Ar+^{51}Cr$	^{38}Ar(d)
13	271	^{49}Cr		43	782	$^{50}Cr+^{39}K$	^{39}K(d)
14	278	^{197}Au	b	44	804	^{50}Mn	f
15	300	^{181}Ta	a	45	809	^{42}Ca	d
16	307	^{48}V	^{48}Cr(EC)	46	811	$^{42}Ca+^{49}Cr$	^{42}Ca(d)
17	315	^{51}Cr		47	830	u	
18	345	^{39}K	d	48	849	^{41}K +	d
18a	358	^{181}Ta	e, a			^{52}Cr	$^{52}Mn(\beta^+, EC)$
19	376	^{53}Mn	$^{53}Fe(\beta^+, EC)$	49	869	^{52}Mn	
20	381	^{42}Ca	d	50	886	^{39}K	d
20a	410	^{54}Fe	e	51	888	^{46}Ti	
21	415	^{181}Ta	a	52	901	^{51}Mn	
22	427+430	$^{48}V+^{51}Mn$		53	909+917	^{42}Ca	d
23	435	^{42}Ca	d	54	928	^{52}Mn	
24	450	$^{197}Au+^{41}Ca$	b+d, resp.	55	934	^{52}Cr +	$^{52}Mn(\beta^+, EC)$
24a	470	u	e			^{197}Au	b
25	477	^{49}Cr		56	937	^{49}Cr	
26	501	^{197}Au	b	57	943	u	e
27	511	$m_e c^2$		58	962	u	
28	546	^{197}Au	b	59	982	^{48}Ti	$^{48}V(\beta^+, EC)$
29	575	^{197}Au	b	60	992	^{36}Ar	d

a: from collimators (Coulex).
b: from target backing (Coulex).
c: background activity.
d: from Si+O, O-contaminant.
e: not well defined in Fig. 6, but seen at other energies.
f: doubtful.
u: unknown.
SE(DE): single (double) escape.

TABLE VI. Same as Table V, but for higher energy γ-rays.

No.	E_γ (keV)	source	Notes	No.	E_γ (keV)	Source	Notes
61	1010	^{53}Fe		91	1512	^{41}K	d
62	1014	u		92	1517	u	
63	1020	^{49}V		93	1524	^{42}Ca	d
64	1062	u		94	1581	^{50}Cr	
65	1097	^{50}Cr		95	1595	^{50}Cr	
66	1106	^{48}Cr		96	1609	^{41}Ca	d
67	1120	^{53}Mn+^{46}Ti	+^{214}Po(c)	97	1628	^{49}Cr	
68	1128	^{54}Fe+^{39}K	^{39}K(d)	98	1642	^{38}Ar+^{42}Ca	d
69	1148	^{47}V		99	1677	^{41}K	d
70	1162	^{51}Cr		100	1762	^{51}Mn+^{35}Cl	^{35}Cl(d)
71	1175	^{49}Cr					+^{214}Po(c)
72	1226	^{42}Ca	d	101	1774	^{39}K	d
73	1240	^{49}V		102	1778	^{28}Si	inel. sc.
74	1250	^{51}Mn+^{53}Mn		103	1787	^{39}K	d
75	1281	^{50}Cr		104	1792	^{39}K	d
76	1289	^{49}Cr+^{46}Ti		105	1821	^{38}Ar	d
77	1292	^{41}K	d	106	1970	^{36}Ar	d
78	1320	^{47}V		107	2038	^{52}Mn	
79	1328	^{53}Fe		108	2150	u	
79a	1333	^{52}Cr	^{52}Mn, e	109	2168	^{38}Ar	+^{38}K(β^+),d
80	1340	^{39}K	d	110	2177	u	
81	1344	^{46}Ti+^{42}Ca	^{42}Ca(d)	111	2209	^{38}Ar	d,+^{214}Po(c)
82	1408	^{54}Fe +	+^{214}Po(c)	111a	2246	^{35}Cl	d,e
		^{39}K	d	112	2303	^{42}Ca	d
83	1415	^{52}Mn+^{49}Cr		112a	2340	^{55}Fe	e
84	1433	^{52}Cr	^{52}Mn(β^+, EC)	113	2489	^{39}K	d
85	1440	^{53}Mn		114	2555	^{42}Ca	d
86	1460	^{40}Ar	c	115	2575	^{39}K	(DE), d
87	1467	^{51}Mn+^{41}K	^{41}K(d)	116	2615	^{208}Pb	c
88	1479	^{51}Cr		117	2647	^{35}Cl+^{38}K	d
89	1499	u		118	2691	^{41}Ca	(SE), d
90	1503	u					

a: from collimators (Coulex).
b: from target backing (Coulex).
c: background activity.
d: from Si+O, O-contaminant.
e: not well defined in Fig. 6, but seen at other energies.
f: doubtful.
u: unknown.
SE(DE): single (double) escape.

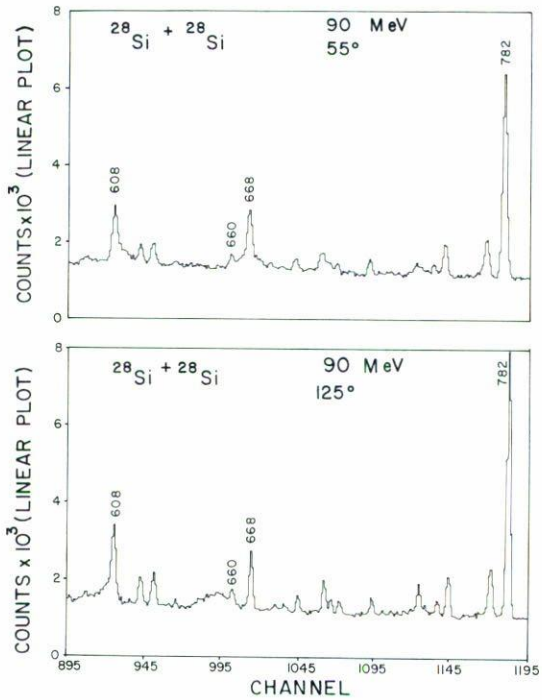

FIGURE 7. Illustration of Doppler-shift effects.

was mentioned before. Spectra of ^{28}Si+^{12}C were also analyzed in order to discard the possibility of carbon contamination and a spectrum taken with a Au target was used to identify the Coulomb excitation lines from the Au backing. The final identification is presented in Tables V and VI, where the origin of the lines not coming from the specific reaction ^{28}Si+ ^{28}Si is indicated.

No large Doppler-shift effects were expected in our spectra since the target backing acts as a stopper for the residues in the reaction. As a rough estimation, we calculated that a residue moving with the center of mass velocity corresponding to the minimum beam energy used in the experiment ($\sim$ 60 MeV) would take about 0.015 ps to traverse the target ($\sim$ 1500 Å). This time (which can reasonably be taken as representative of the maximum time of flight of the residues before entering the Au-stopper) is smaller than all the known lifetimes for the transitions of interest in the actual residues. In addition, it is usually the case that most or all the ground state transitions are actually the final members of a γ-ray cascade, being thus further dalayed with respect to the moment at which the reaction ocurred. We might then expect that most of the γ-rays are emitted when the residue is at rest, and that this assumption will be most reliable for the transitions of most interest in our experiment.

Several spectra were taken with the detector placed at 55° in order to check these expectations experimentally. Since the angular distributions are symmetric with respect to 90° [see formula (4)], the only difference that might be expected in these spectra is an inverted Doppler shift of the peaks because of the opposite velocity components of the fragments with respect to the detector. This effect was actually seen in the five $\theta = 55°$

TABLE VII. γ-ray lines analyzed in ^{28}Si+ ^{28}Si. The energies of the lines used to obtain the total cross sections for each element are given in column 2 while other lines that were analyzed are listed in column 3.

Residue	E_γ (keV) (main)	E_γ (keV) (also analyzed)
^{46}Ti(2α2p)	888[a]	1120, 1289
^{47}V(2αp)	1148	1320
^{48}V(α3pn)	427 + 626[b]	199, 307
^{48}Cr(α2p2n)	751	1106
^{49}V(α3p)	1021	1241
^{50}Cr(α2p)	782[a]	1098, 1283, 1582, 1597, 609, 661
^{51}Cr(4pn)	1163 + 1480	314
^{51}Mn(αp)	237[c] + 1139[b]	901, 1250
^{52}Mn(3pn)	869	620, 2038
^{53}Mn(3p)	1440	1120, 1250
^{53}Fe(2pn)	700[c]	1328, 2340, 1010
^{54}Fe(2p)	1409[a]	

(a) A contribution from ^{28}Si+^{16}O was subtracted (see text).

(b) This determination involves reported branching ratios (see text).

(c) A correction for activity from a long lived state was made (see text).

spectra taken at bombarding energies of 75, 80, 85, 90, and 95 MeV, which showed a slight broadening of the right side of some peaks in contrast to the left-side broadening observed in the original $\theta = 125°$ spectra.

This is illustrated in Fig. 7, where corresponding portions of two spectra taken at symmetric angles at the same bombarding energy are shown. The line at 660 keV, corresponding to the highest lying transition observed in ^{50}Cr, shows a broad hump at its left or right for the 125° or 55° spectrum, respectively. Since the decaying level is short lived in this case (reported lifetime of < 0.14 ps), the large effect here observed (actually the largest seen, by far) is in agreement with our expectations. The sharp peak still seen at 660 keV may be an unshifted component of the same line or could correspond to a different transition, for which a good candidate is the $(6)^+ - 6^+$ transition in ^{50}Cr, fed by the β-decay of ^{50}Mn.

Examples of moderate and negligible Doppler shift effects, more typical in our spectra, are provided by the 608 keV and 782 keV lines, respectively, as shown in Fig. 7. Here again, the strength of the effect can be related to the relevant lifetimes (0.6 ps and 9 ps, respectively) and to the corresponding positions in the γ-ray cascade (second highest lying transition and ground state transition in ^{50}Cr, respectively). After all the lines that were actually analyzed in our experiment were carefully checked for Doppler shifts, we decided that no special provision was necessary in the analysis to account for this effect.

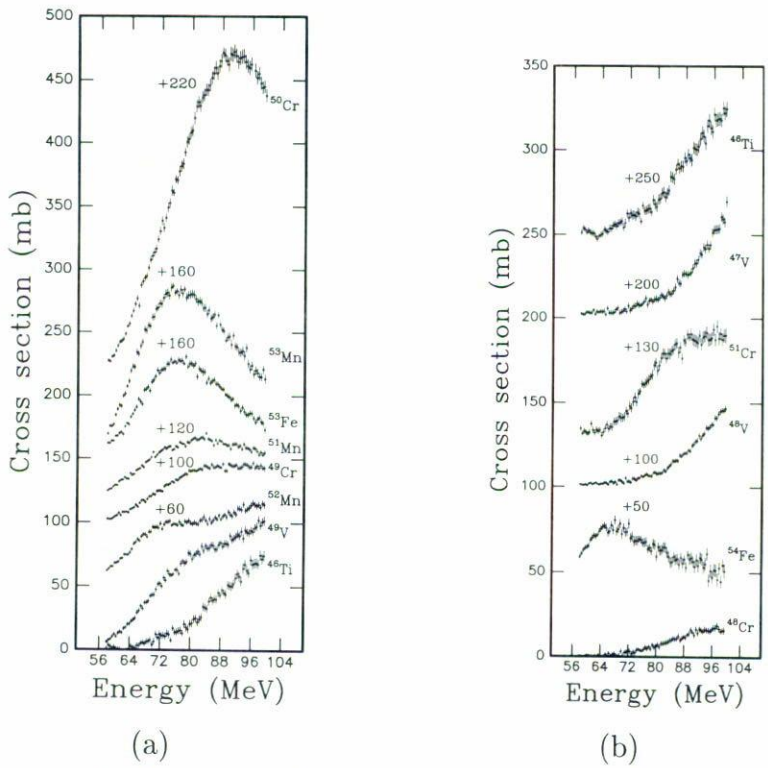

FIGURE 8. Excitation functions for (a) the eight more prominent and (b) the six less prominent evaporation channels observed in the ^{28}Si+ ^{28}Si reaction.

The γ-ray lines used to determine the production cross sections for the reaction residues are indicated in the second column of Table VII, while the most probable evaporated particles are indicated in parentheses following the name of the element, in column 1. As a test of consistency, the excitation functions for higher lying transitions were also studied whenever possible. These are listed in the third column of the Table VII. The excitation functions for the different evaporation channels are shown in Figs. 8a and 8b. This last figure includes five additional evaporation channels not presented in Ref. 9 or elsewhere.

8. CONCLUSIONS

The gamma-ray technique has been illustrated through an exhaustive analysis of data taken for the ^{28}Si+ ^{28}Si fusion reaction. Careful classification of all the observed gamma-ray lines led to the positive identification of thirteen evaporation channels. The excitation functions for five of these channels were presented here for the first time.

Special emphasis was given to the absolute normalization procedure, which actually provides a method to determine the thickness of thin targets deposited on thick backings. Even though this thickness determination might not be as precise as that obtained

with other methods [22], we showed that in the absolute normalization factor the errors resulting from inaccurate charge collection are approximately cancelled due to their expected bias toward positive values and to the fact that only ratios of charges appear in the scaling formula.In other words, even though the procedure may give fairly large errors for target thickness determinations (rows 1 and 3 of Table II), it does give precise enough results for absolute cross sections (rows 2 and 4 of Table II).

Among the advantages of the technique are the relative ease of obtaining high statistical accuracy and the clean separation that can be made of the individual evaporation products. The major disadvantage is the fact that residual nuclei which are formed in the ground state (or in a long lived isomeric state) either directly by particle evaporation or via high-energy γ-ray transitions cannot be observed.

REFERENCES

1. D.A. Bromley, (Ed.), *Treatise on Heavy-Ion Science*, Vols. 1 to 7 (Plenum, New York, 1984).
2. R.G. Stokstad, Y. Eisen, S. Kaplanis, D. Pelte, U. Smilansky, and I. Tserruya, *Phys. Rev. Lett.* **47** (1978) 465.
3. E.F. Aguilera, J.J. Vega, and J.J. Kolata, *Rev. Mex. Fís.* **4** (1997) 622.
4. F.S. Stephens, N.L. Lark, and R.M. Diamond, *Nucl. Phys.* **63** (1964) 82.
5. J.O. Newton, *Progr. Nucl. Phys.* **11** (1970) 53.
6. T. Nomura, H. Morinaga, and B. Povh, *Nucl. Phys. A* **127** (1969) 1.
7. J.J. Kolata, R.A. Racca, P.A. DeYoung, E. Aguilera Reyes, and M.A. Xapsos, *Phys. Rev. C* **32** (1985) 1080.
8. E.F. Aguilera, Ph.D. Dissertation, University of Notre Dame (1985).
9. E.F. Aguilera, J.J. Kolata, P.A. DeYoung, and J.J. Vega, *Phys. Rev. C* **33** (1986) 1961.
10. R. Pengo, *Nucl. Inst. and Meth* **B56/57** (1991) 933.
11. Gamma Ray Energies and/or Branching Ratios can be found in: *I. Tables Ordered by γ-Energy and/or by nuclide*: 1. (A = 6 to A = 20) R.J. de Meijer and H.S. Plendl, *At. Data and Nucl. Data Tables* (ADNDT)**13** (1974) 1; 2. (A = 21 to A = 32) R.J. de Meijer, A.G. Drentje, and H.S. Plendl, ADNDT **15** (1975) 391; 3. (A = 33 to A = 44) R.J. de Meijer and A.G. Drentje, ADNDT **17** (1976) 211; 4. (A = 32 to A = 46) E.K. Warburton, J.J. Kolata, J.W. Olness, A.R. Poletti, and P. Gorodetzky, ADNDT **14** (1974) 147; *II. Energy-Level Schemes*: 1. (All A) Eds. C.M. Lederer and V.S. Shirley, Table of isotopes, seventh edition, (Wiley, 1978); 2. (A = 18 to 20, but with references to all A) F. Ajzenberg-Selove, *Nucl. Phys. A* **392** (1983) 1; 3. (A¿44, but with references to all A) Nuclear Data Sheets, each issue has a cumulative index to A-chains; 4. (A = 21 to 44) P.M. Endt and C. Van der Leun, *Nucl. Phys. A* **310** (1978) 1.
12. N. Tsoulfanidis, *Measurement and Detection of Radiation*, (McGraw Hill, New York,1983).
13. K. Debertin and R.G. Helmer, *Gamma and X-Ray spectrometry with semiconductor detectors*, (North Holland, 1988).
14. L.A. McNelles and J.L. Campbell, *Nucl. Inst. Meth.* **109** (1973) 241.
15. J.J. Kolata, R.M. Freeman, F. Haas, B. Heusch, and A. Gallman, *Phys. Lett.* **65B** (1976) 333.
16. K. Alder and A. Winther, Reprints on Coulomb Excitation, *Perspectives in Physics*, (Academic Press, New York, 1966).
17. P.A. DeYoung, Ph.D. Dissertation, University of Notre Dame (1982).

18. H.J. Rose and D.M. Brink, *Rev. Mod. Phys.* **39** (1967) 306.
19. M.A. Van Driel, H.H. Eggenhuisen, G.A.P. Engelbertink, L.P. Ekstrom, and J.A.J. Hermans, *Nucl. Phys. A* **272** (1976) 466.
20. T. Yamazaki, *Nucl. Data* **3** (1967) 1.
21. G.A.P. Engelbertink, L.P. Ekstrom, D.E.C. Scherpenzeel, and H.H. Eggenhuisen, *Nucl. Inst. Meth.* **143** (1977) 161.
22. E.F. Aguilera, E. Martinez-Quiroz, H.M. Berdejo, and M.C. Fernandez, *Rev. Mex. Fís.* **41** (1995) 507.